Chapter

Mode Interpretation of Aerodynamic Characteristics of Tall Buildings Subject to Twisted Winds

Lei Zhou and Kam Tim Tse

Abstract

Hills alter wind properties not only by accelerating the wind flow but also by changing the flow direction. Therefore, the wind profile near mountainous terrain continuously exhibits both wind speed and wind direction variation along with the vertical height, and is generally referred to as a twisted wind profile (TWP). The aerodynamic properties of the tall building exposed to TWP are significantly different from those exposed to a conventional wind profile (CWP) and thus generate the twisted-wind effect. The spatial–temporal aerodynamic feature of a tall building under unsteady wind is highly complicated, and the associated flow field is a random and obscure high-dimensional dynamic system. To elucidate the fundamental mechanism involved in TWP, principal orthogonal analysis (POD) is employed to identify the pressure and flow patterns. Moreover, the extracted modal features can be used to physically interpret the coherent structure and dynamical patterns hidden in the surface pressure field or the turbulent flow field. This mode interpretation of aerodynamic characteristics of tall building provides a better understanding of the underlying mechanism of the twisted-wind effect.

Keywords: mode interpretation, aerodynamic properties, pressure pattern, flow pattern, spatial–temporal feature, twisted-wind effect, POD; tall building

1. Introduction

Due to nonuniform geometric features of mountainous topography (e.g., slope and curvature), hills can significantly modify wind properties not only by accelerating the wind flow but also by altering the flow direction. As a result, wind profiles in the proximity of hills exhibit both wind speed and direction variation with height, which are generally referred to as twisted wind profiles (TWP), as shown in **Figure 1** [1–4]. Tall buildings built in hilly landforms, such as in Hong Kong and Japan, have a high probability of being attacked by the topography-induced twisted wind. The varying wind directions in a twisted wind profile can produce a highly non-uniform flow field around a building. Exhibiting varying degrees of flow separation and reattachment as well as
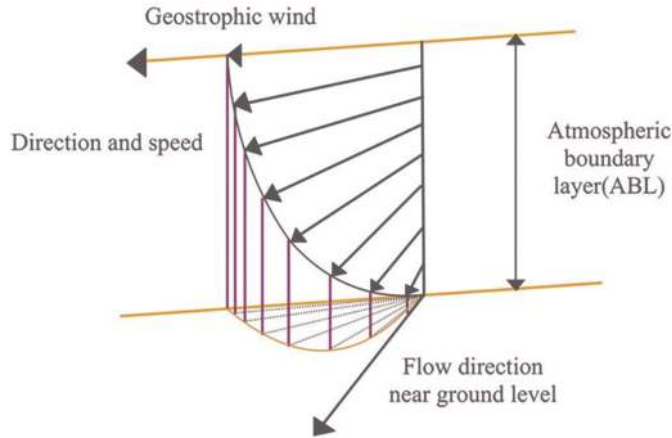
Figure 1.
Schematics of twisted wind (TWP).

varying vortex structures along with the building height. A non-uniform flow field can induce irregular pressure distribution on the external walls of a building and, thus, asymmetric wind loads. Asymmetric wind loads can increase the torsional loading and hence affect sway and twist responses, which are usually only minor considerations when designing buildings in conventional wind profiles. In addition, an increased correlation between wind load components will occur because the wind turbulence associated with a twisted wind profile spans from the windward face to the side face along with the height of a building as a result of the changing wind angles [5–8]. Thus, in comparison to the conventional wind profile (CWP), the aerodynamic characteristics and flow field in the presence of TWP become more complicated, forming a random and nonlinear high-dimensional dynamic system with obscure and elusive features [9, 10].

Therefore, it is of great importance to conduct a deep and systematic investigation on the pressure patterns and flow patterns of tall buildings exposed to the twisted wind instead of only focusing on the micro aerodynamic features but neglecting to reveal the mechanism. This approach is expected to provide a better understanding and physical interpretation of the twisted-wind effect; thus, it can further provide theoretical guidance to ensure wind safety and to optimize the control measures of wind-induced responses for tall buildings built in mountainous terrain.

To extract the spatial-spectral features and dynamic characteristics from the random pressure field, reduced-order models (ROMs) are recommended as an effective way [11, 12]. The goal of ROMs is to search for a relatively straightforward low-dimensional system to represent a chaotic, high-dimensional system through a process of decomposition, truncation, and error estimation [13]. As one of the most typical and effective ROMs models, Proper Orthogonal Decomposition (POD) is a multivariate statistical technique that aims to extract the dominant patterns from the inter-correlated and dependent original observations [14]. The principle of POD is to find a set of the optimal orthogonal bases called principal components in a second-order statistic sense, and then describe the important information by the superposition of the product of the POD base and modal coefficients [15]. POD has numerous advantages like extracting the most important information, compressing the data dimensionality, eliminating noise interference, and more importantly, identifying the structures and patterns contained in the seemingly disordered original observations. As a result, POD has been widely and successfully applied in the fields of both fluid

mechanics and wind engineering to capture coherent structures and pressure patterns contained in the flow field and the associated pressure field [16–19]. However, almost all previous studies have only addressed the topic regarding modal identification of the aerodynamic characteristics of tall buildings exposed to conventional wind profiles, Barely no study to date examines that under TWP [20, 21]. It is evident that the aerodynamic properties under TWP are significantly changed and they are not be simply equivalent to the case of CWP with a certain wind incident angle. Thus, it is necessary to identify the coherent structure and interpretate the structures hidden in the aerodynamic features of a tall building, specifically for twisted wind. Additionally, the POD technique is believed to facilitate deep understanding and physical insight into the unique flow and pressure patterns in the presence of twisted wind. This mode interpretation tool is thus helpful to elucidate the underlying aerodynamic interaction mechanism between TWP and tall buildings.

The remaining parts of this paper are organized as follows. Section 2 introduces the methodology of POD and the related notion/notations. Section 3 describes how we used wind tunnel testing and numerical simulation methods to obtain wind pressure and flow field data; Section 4 illustrates the POD analysis results on the wind pressure, and compares the pressure pattern between CWP and TWP cases; Section 5 shows the POD analysis results on the flow field, and compares the flow patterns between CWP and TWP cases. Section 6 gives concluding remarks on the mode interpretation of the aerodynamic characteristics of tall buildings subject to twisted winds as well as recommendations on future work.

2. Methodology

A brief description of the POD principle for the velocity/pressure field is presented here, and more details about the theoretical derivation and practical application can be found in [19].

For moment t_i, velocity or pressure components $f_i(x_m)$ at a monitored location m are arranged in a vector q_i to formulate a snapshot, the total number of velocity snapshots N with sampling interval Δt can then be assembled in matrix Q_N. The Time-average field $\overline{Q}$ should be firstly subtracted from the instantaneous velocity or pressure field to obtain the zero-centered fluctuating matrix Q'_N.

$$q_i = \begin{bmatrix} f_i(x_1) \\ f_i(x_2) \\ \vdots \\ f_i(x_m) \\ \vdots \\ f_i(x_M) \end{bmatrix} \tag{1}$$

$$Q_N = [q_1, q_2, q_3 \cdots q_N] \tag{2}$$

$$Q'_N = Q_N - \overline{Q} \tag{3}$$

Where $\{x_1 \ x_2 \ \cdots \ x_m\}$ signify the position of the monitored mesh points, and M is the total number of the monitored points.

The purpose of POD is to determine a set of orthogonal bases, and equivalently express q_i' as the superposition of the product of the POD base and corresponding modal coefficients.

$$q_i' = \sum_{k=1}^{n} a_{ki} \varphi_k \tag{4}$$

To identify POD basis, a covariance matrix C is formulated as $C = Q_N'^T Q_N'$, and the eigenvalue and eigenvector can be obtained by solving the eigenfunction of matrix C as follows,

$$C\varphi_k = \lambda_k \varphi_k \tag{5}$$

where the eigenvalue λ_k reflects the energy contribution of each POD mode and is arrayed in descending sequence, eigenvector φ_k represents the POD modes and any two of them are orthogonal to each other spatially.

Modal coefficients $A = [a_{ki}] \, (k = 1, 2, 3 \cdots n; \quad i = 1, 2, 3 \cdots N)$ are determined by projecting the original fluctuating velocity or pressure field onto the POD modes as follows,

$$A = \Phi^T Q_N' \tag{6}$$

where the spatial POD mode $\Phi = [\, \varphi_1 \quad \varphi_2 \quad \ldots \quad \varphi_n \,]$ and the temporal modal coefficient $A = [a_{ki}] \, (k = 1, 2, 3 \cdots n; \quad i = 1, 2, 3 \cdots N)$.

3. Data resources

3.1 Wind pressure data resources

Pressure measurement testing was carried out on a rectangular tall building, of cross-Section 180 mm × 60 mm (Breadth×Depth) and height of H = 600 mm. The pressure distribution on the 1:400 scaled building model was measured using a DSM3400 synchronous multi-pressure sensing system (SMPSS). **Figure 1** shows arrangement details of the pressure taps and experimental setup. Pressure taps were arranged in 14 rows ×12 columns on the windward/leeward surfaces and in 14 rows ×4 columns on side surfaces. The sampling frequency and duration were 330 Hz and 90 s respectively. In this study, the approaching wind perpendicularly attacking the relatively wider and narrower surface of the building correspond to two different working conditions, i.e., angle of attack (AOA) of 0 degree and 90 degrees respectively.

The three targeted wind profiles have similar distributions of velocity and turbulence but different twisted angle profiles. Specifically, the wind speed and turbulence intensity profiles follow power-law functions with exponents of 0.11 and − 0.24. The maximum twisted angles are 0°, 15° and 30°, thus the profiles are respectively labeled CWP, TWP15 and TWP30. It should be noted that variation of twisted angles with height for TWP15 and TWP30 conforms with the negative power curve expressed in Eqs. (7) and (8), and as given in [22].

$$\theta_{15}(z) = 15 \times \exp\left(-0.0976 \times (z/25)\right) \tag{7}$$

$$\theta_{30}(z) = 30 \times \exp\left(-0.106 \times (z/25)\right) \tag{8}$$

where $\theta_i(z)$ represents the twisted angle measured at the height z; the subscript i denotes the maximum twisted angle of TWP, herein, i = 15 and 30.

Three types of wind fields (CWP, TWP15 and TWP30), were generated in a wind tunnel by using passive simulating facilities. As shown in **Figure 2(b)** and **(c)**, to replicate the twisted wind, the wooden vane system was placed 5 m upstream away from the central axis of the building model, and the windward ends of the single wooden vane were isolated 1 m from each other. It should be noted that the wooden vane employed in this study was adjustable, indicating that the wooden strip at a certain height could be offset at any desired angle. Moreover, to compensate for the dissipation near the wind tunnel ground, three rows of roughness elements were rotated at a certain angle are set in a stagger arrangement and placed between the wooden vane

Figure 2.
Experimental setup and details: (a) distribution of pressure taps on building model; (b) TWP test arrangement in wind tunnel; (c) section plan of the experimental setup.

system and the building model. To determine the region with uniform twisted flow properties, a grid measurement system constituted by blue dash lines was utilized to monitor the flow features at each grid point. After trial and error, it turned out that the targeted twisted wind can maintain consistent flow properties within a rectangular region (shaded in orange) with dimensions of 1.5 m × 2.0 m (width ×length) around the turntable center. z_{ref} indicates the reference height which is located at the building roof (z = 0.6 m); U_{ref} denotes the reference velocity and equals 6.2 m/s; I_{ref} represents the reference turbulence intensity and equals 6.9%. According to the reference wind speed U_{ref} and building breath B, the Reynolds number is calculated as Re = 2.55 × 10^4.

3.2 Flow field data resources

3.2.1 Inflow turbulence generation

Appropriately replicating the inflow turbulence features is a requisite for obtaining accurate LES simulation results. In this study, the narrowband synthesis random flow generator (NSRFG) technique is utilized to simulate inflow turbulence by generating time history series of the fluctuating velocity. Turbulence integral scales (see Eqs.(9)– (11)) conform to those in wind codes (AIJ, 2004; ESDU 85020, 2001), which are also identical to the setting given in [7]; the velocity distribution in the frequency domain corresponds to the von Karman spectrum (see Eqs. (12)–(14)), which can reflect typical spectral features of the turbulent ABL flow in a wind tunnel. The superimposition of the zero-mean fluctuating component and the mean wind profile formulate the initial inflow boundary condition. For specific implement procedures, one can refer to the work of [23]. Note that the profiles of wind speed, turbulence intensity and twisted angle are consistent with the setting in the wind tunnel.

$$L_u(z) = 100 \cdot \lambda_L \cdot \left(\frac{z}{30\lambda_L}\right)^{0.5} \tag{9}$$

$$L_v(z) = 0.5\left(\frac{\sigma_v}{\sigma_u}\right)^3 L_u(z) \tag{10}$$

$$L_w(z) = 0.5\left(\frac{\sigma_w}{\sigma_u}\right)^3 L_u(z) \tag{11}$$

$$S_u(f) = \frac{4(I_u U)^2 (L_u/U)}{\left[1 + 70.8\left(fL_u/U\right)^2\right]^{5/6}} \tag{12}$$

$$S_v(f) = \frac{4(I_v U)^2 (L_v/U)\left[1 + 188.4\left(2fL_v/U\right)^2\right]}{\left[1 + 70.8\left(2fL_v/U\right)^2\right]^{11/6}} \tag{13}$$

$$S_w(f) = \frac{4(I_w U)^2 (L_w/U)\left[1 + 188.4\left(2fL_w/U\right)^2\right]}{\left[1 + 70.8\left(2fL_w/U\right)^2\right]^{11/6}} \tag{14}$$

where λ_L is the scaled ratio; $L(z)$, $I(z)$ and $S(z)$ are the turbulence integral scale, turbulence intensity and power spectral respectively. The subscripts u, v and w denote

the components of the physical quantities in the along-wind, crosswind, and torsional directions respectively; f is the frequency.

3.2.2 Numerical simulation details

The computational domain and boundary conditions are illustrated in **Figure 3**. The building model is scaled to 1/400 with dimensions of 180 mm (breadth) $\times$ 60 mm (depth) $\times$ 600 mm (height) and set as wall condition. The calculation domain covers the ranges of 20H in the streamwise direction, 16H in the crosswind direction and 8H in the vertical direction. In this study, the wind incident angle of 90 degree exactly corresponds to the side ratio case of 3:1, where the flow phenomenon is more complex.

The structured hexahedral grids were utilized to mesh the outer calculation domain, while for the inner region, an O-shaped grid with good orthogonality was employed. Additionally, local mesh refinement was performed near the building surface and wake region to better capture the significant features of the shear layer and recirculation zone. For example, 10 layers were imposed on the building wall to simulate the near-wall velocity gradient. The normal growth rate of the mesh within the boundary layer was 1.02, while for the grids was relatively far away from the external surface boundary, the growth rate was 1.1. To ensure y^+ in the most region was around 1, the distance from the building wall to the center of the first layer was set as $\Delta y/B = 2.0 \times 10^{-4}$. The mesh scheme and distributions around the building are illustrated in **Figure 4**.
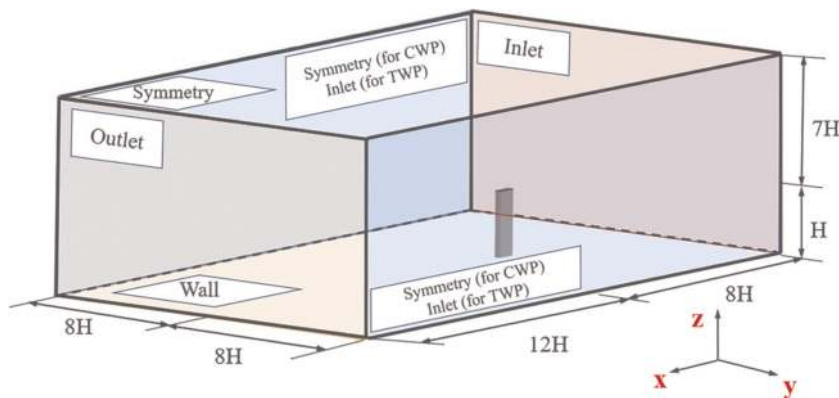
Figure 3.
*The boundary conditions of the computational domain for CWP and TWP.*
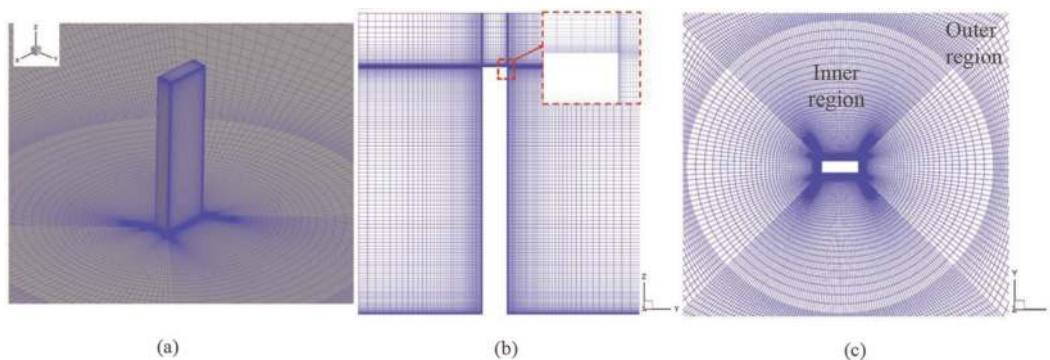
Figure 4.
Mesh scheme and distributions around building: (a) perspective view of 3D mesh distribution; (b) side view of the local 2D mesh (y = 0); (c) top view of the local 2D mesh (z/H = 0.5).

LES with the NSRFG-generated inflow boundary condition was adopted in this study to evaluate the effect of different wind profiles on a tall building. The numerical solver used herein is the commercial CFD code FLUENT. The finite volume method (FVM) was employed to solve the governing equations. SIMPLEC algorithm, initially proposed by [24], was adopted to solve the pressure–velocity coupling scheme. The convection and diffusion terms are discretized using the second-order upwind scheme. The temporal discretization scheme is the implicit time-stepping method. The time step in this paper was set as $\Delta t = 5 \times 10^{-5}$ to ensure the courant number in most calculation region is less than one.

3.3 Validation of the simulated TWP and numerical results

The flow properties of the targeted, experimental and numerical wind profiles at the building location for CWP, TWP15 and TWP30 are compared in **Figure 5**. For better comparison, these three types of wind flow have identical wind speed and
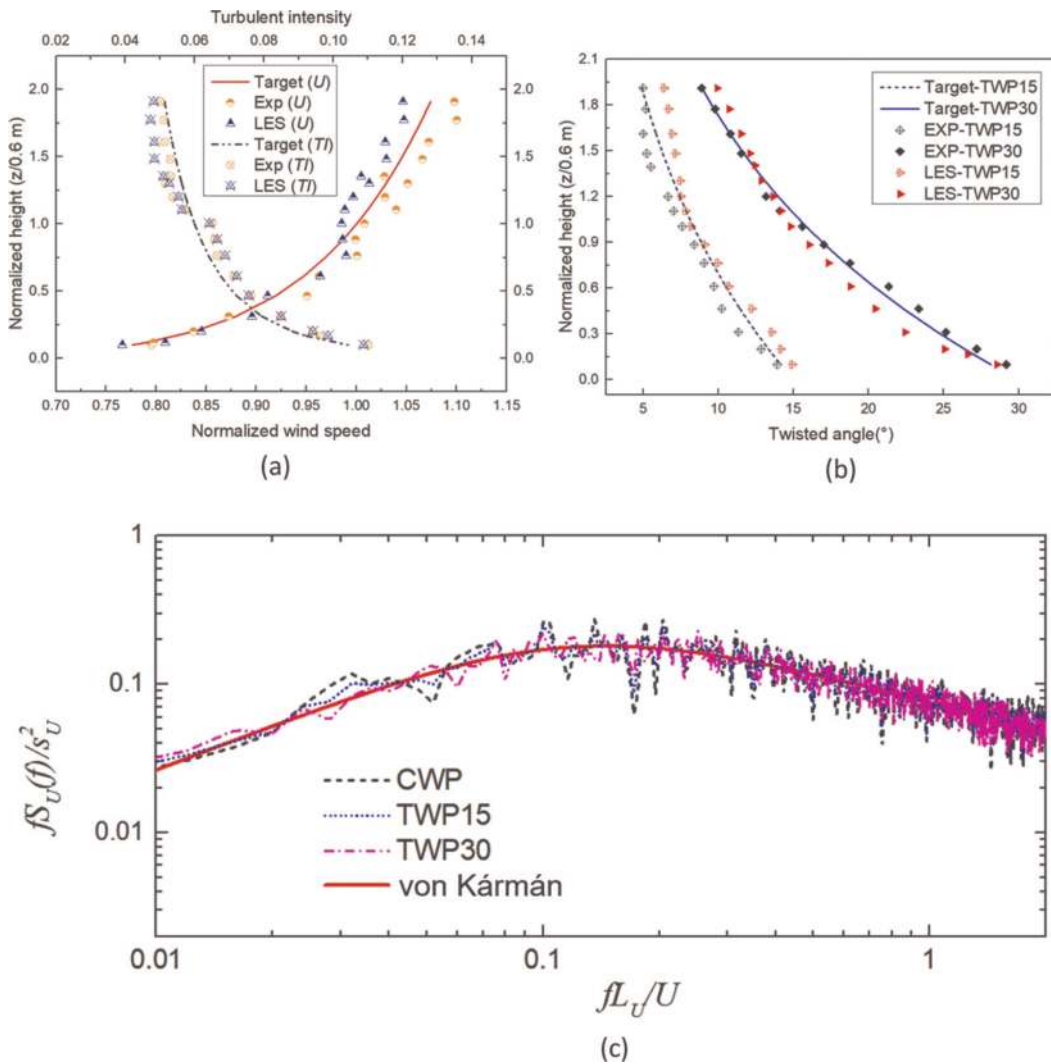
Figure 5.
Flow properties of the targeted, experimental and numerical wind profiles at the location of building for CWP, TWP15 and TWP30: (a) normalized wind speed and turbulent intensity profile; (b) twisted angle profile; (c) power spectrum.

turbulence intensity profile but different twisted angle profiles. Thus, only one set of data is provided in **Figure 5(a)**. Evidently, both the numerically and experimentally replicated wind profiles agree well with the targeted result. The simulated twisted wind conditions, TWP15 and TWP30, had the largest twisted angle at the ground level, which is about 15°and 30°, and both of them well conformed to the targeted variation trend in the vertical direction as expressed in Eqs. (7) and (8). The longitudinal wind velocity spectrum at the reference height is in good agreement with the von Karman spectrum within a relatively wide scope, including the inertial subrange, as shown in **Figure 5(c)**.

The distribution of the pressure coefficients along the circumference of the building at a height of z = 2/3H obtained by LES and wind tunnel test are compared in **Figure 6** for cases CWP and TWP30. Affected by twisted flow, the location of the largest positive pressure and stagnation point is moved towards the right-side of the building on the windward side. When exposed to CWP, the pressure distributions on the left- and right- side surfaces of the building are symmetrical, while under TWP, significant differences are noted both for mean and fluctuating coefficients. The most distinctive discrepancy of the mean pressure between CWP and TWP30 occurs at the right-side surface of the building, simply because it becomes partially windward when the building is exposed to the twisted wind. A similar phenomenon can also be observed for the fluctuating pressure with the largest difference 86.84% appearing at monitoring point 22. Notably, wind twisting can significantly magnify the mean C_p while greatly weakening the fluctuating C_p on the right-side surfaces.

Generally, the pressure distribution obtained in LES at 2/3 height of building shows reasonably good agreement with its counterpart in wind tunnel testing, especially for mean Cp. As a result, although small discrepancies exist, the numerical methods used in this study can still provide reliable and reasonable results for the evaluation of the twisted-wind effect.
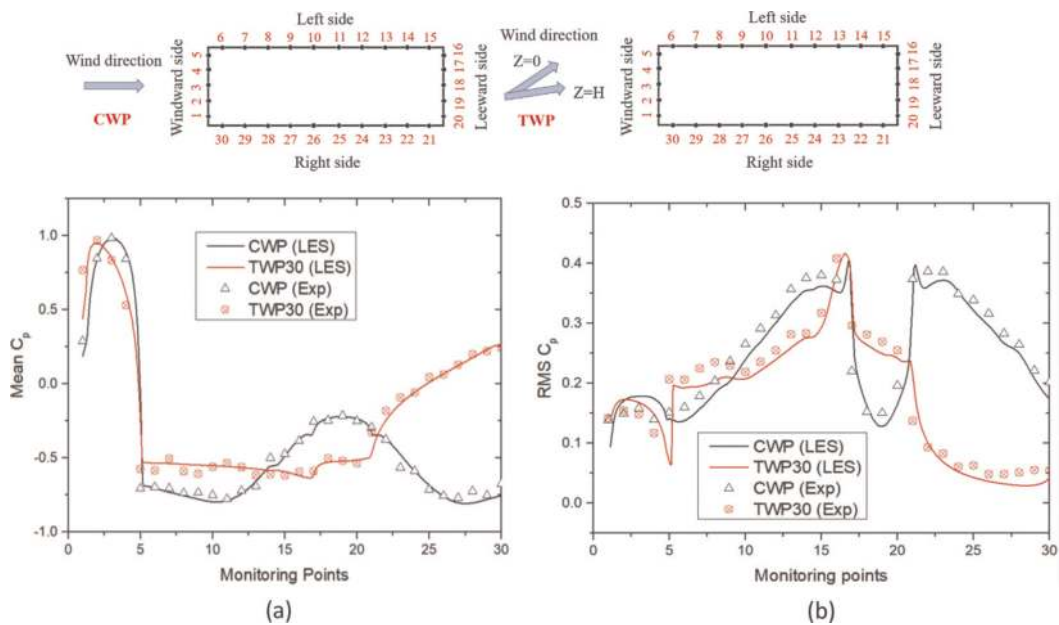
Figure 6.
Mean and fluctuating pressure coefficients at height of z = 2/3H obtained by LES and experiment under CWP and TWP30.

4. POD analysis of surface pressure

The rectangular building with AOA of 0°and 90°represents two different side ratio cases, in which the twisted wind can exert remarkably different effects on the pressure pattern. As a result, to better understand the fluid–structure interaction mechanism, POD was employed to identify the pressure patterns hidden in the fluctuating pressure field on the building surface.

4.1 Mode energy distribution

The energy contributions of the dominant modes and the normalized cumulative number of modes are presented in **Figure 7**. Affected by twisted flow, the fluctuating energy of each pressure mode was reduced to a certain degree, especially for the dominant modes. The energy proportion of the first mode in the case of 0°AOA was larger than that in the case of 90°AOA for the two different flow types CWP and TWP30. Moreover, the difference in the energy percentage between the dominant modes for the case 0° AOA was much more significant in comparison with that of 90° AOA. For example, the fluctuating energy occupied by the first mode of CWP with 0° AOA was around 33%, more than twice that of the second mode. This observation can be attributed to the fact that a tall building with a larger side ratio can produce more complicated flow motion, topology, and behavior. As a result, to reach 90% of the total energy, only the first 5% modes were needed for case 0°AOA, but much larger modes of 24% were needed for the 90° AOA case.

4.2 PSD of the modal coefficients

The power spectral density of the first two POD modes coefficients for the 0° and 90° AOA cases are compared in **Figure 8**. Generally, the twisted flow had a larger effect on the low-frequency region than the high-frequency region for the first mode, while this observation was exactly the opposite for the second mode.

In the case of 0°AOA, as marked by a rectangle in **Figure 8**(a_1), the low-frequency shift mode dominated the first pressure pattern for case CWP while it became less pronounced for case TWP30. The second POD mode of case CWP was distinctively controlled by the vortex shedding phenomenon with the peak appearing at $f_{11} \approx 0.1$.
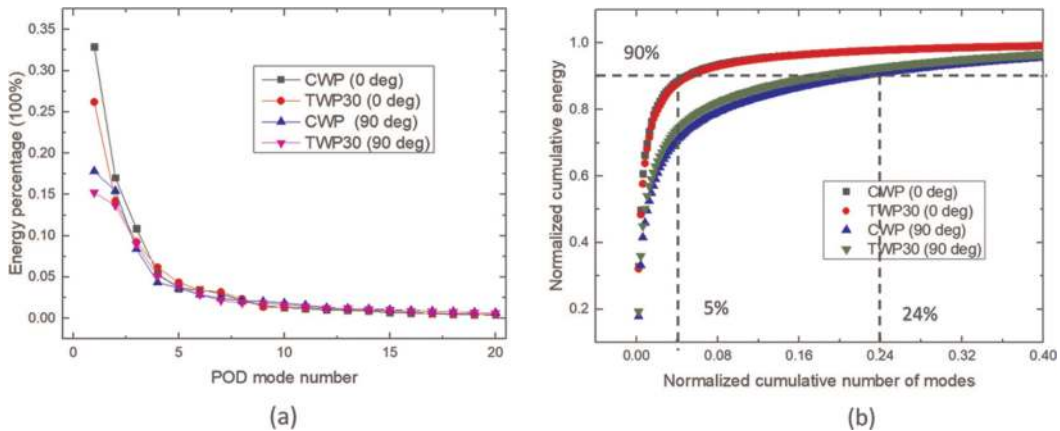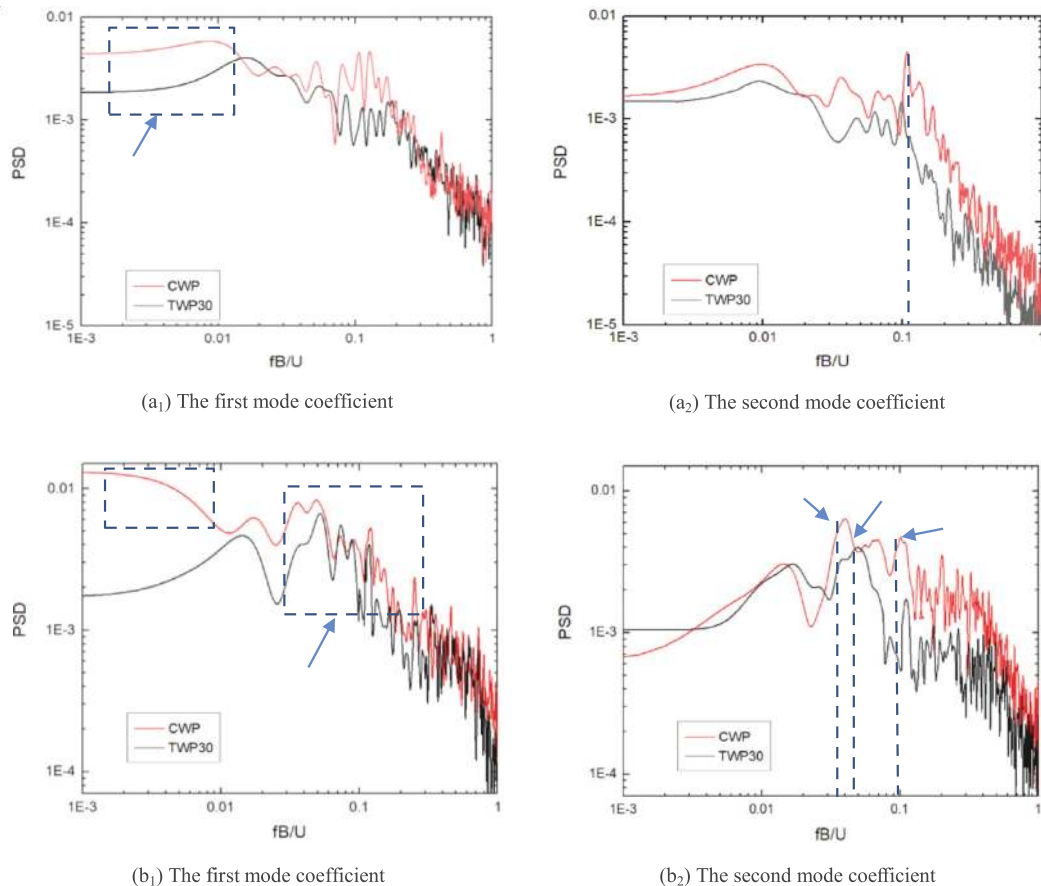

Figure 7.
Energy contributions of (a) dominant modes; (b) normalized cumulative number of modes.

However, the twisted wind reduces this peak energy, indicating that the Karman vortex motion is weakened in the presence of TWP.

In the case of 90°, as shown in **Figure 8**(b_1), although the multi-peak region can be observed in the PSD of the first-order mode for the two wind profiles, it should be noted that the shift mode only appeared in the case of CWP. The second mode under CWP is controlled by two types of vortices shedding behavior with f_{21} = 0.04 and f_{22} = 0.102, and as a result, these two different flow motions around a large aspect ratio building (3:1) can be speculated to be leading-edge vortex shedding (LEVS) and trailing-edge vortex shedding (TEVS) respectively [25]. The existence of twisted flow significantly changes the energy magnitude, the main frequency and the number of peaks. For example, in the case of TWP30, there was only one pronounced peak, whose energy was slightly reduced but the frequency increased to f31 = 0.048. Thus, it is reasonable to surmise that the second mode of TWP 30 is highly related to alternate-edge vortex shedding (AEVS) [25, 26].

4.3 POD pressure pattern

The first two POD modes of the pressure field on the building surface for case CWP and TWP30 with 0°AOA are shown in **Figure 9**. When exposed to CWP, the first mode pattern had a similar distribution with the mean pressure filed on the
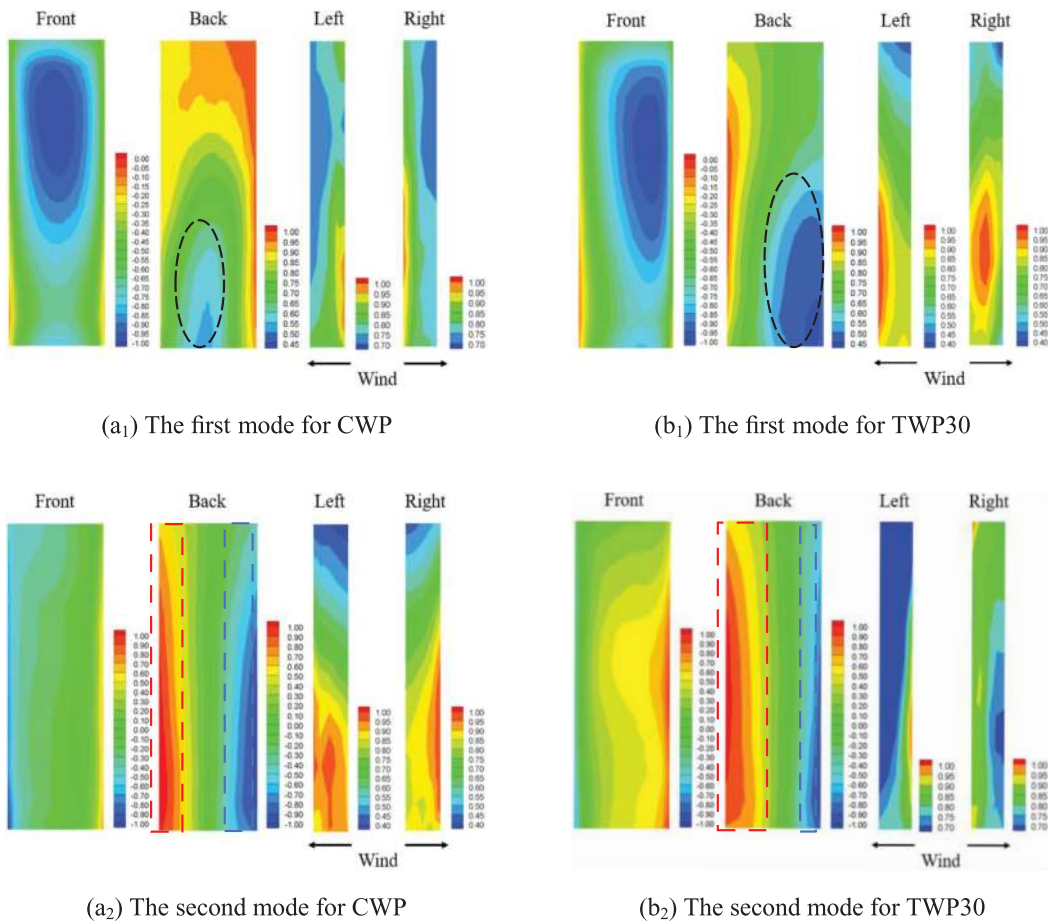

(a$_1$) The first mode coefficient   (a$_2$) The second mode coefficient

(b$_1$) The first mode coefficient   (b$_2$) The second mode coefficient

Figure 8.
Power spectral density of the first two POD mode coefficients for two AOA cases of (a) 0°; (b) 90°.
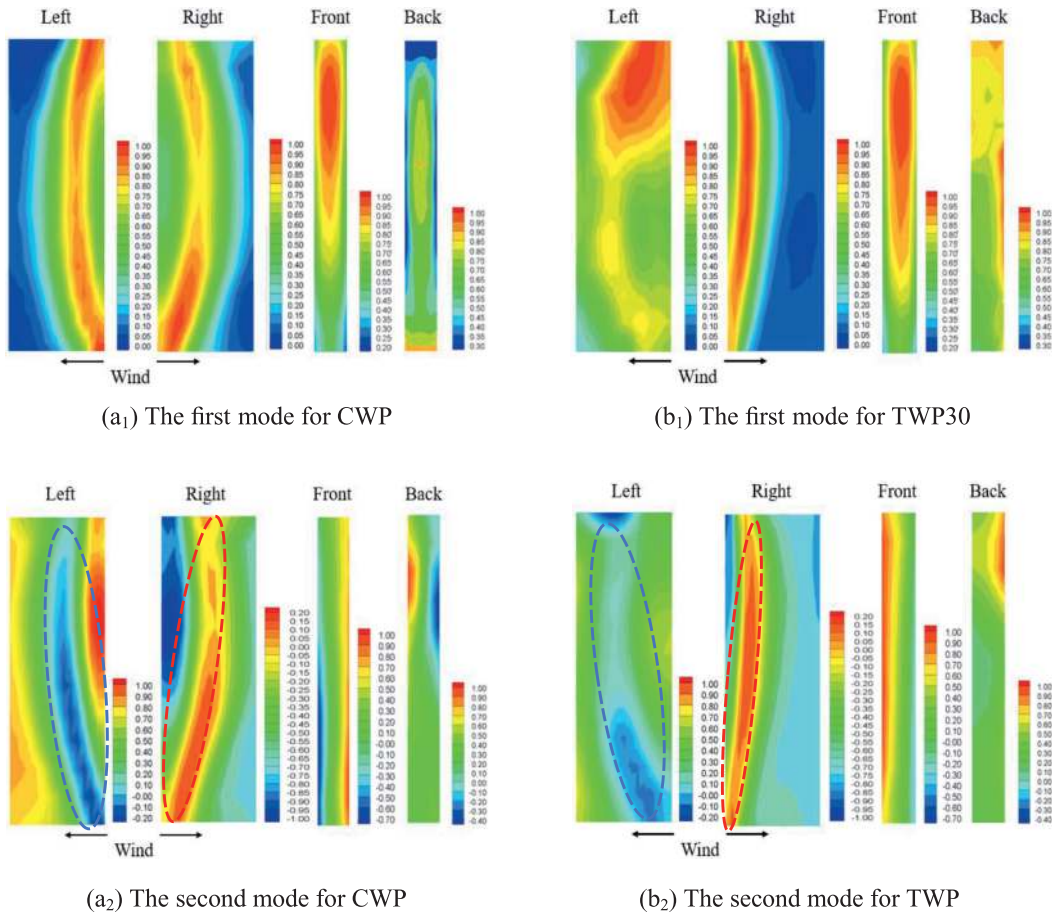
building surface as depicted in **Figure 8**, which implies that the first POD mode possibly corresponds to the low-frequency shift mode. Moreover, it is reasonable to deduce that the second asymmetrical mode shape well captured the fluctuating properties induced by the periodic vortex shedding.

In the presence of twisted wind, the POD mode pattern on the building surfaces became asymmetric and non-uniform. It was evident that the vertical varying wind direction had a noticeable influence on the mode shape on the leeward surface. Specifically, the first mode shape was significantly deflected towards the right side near the downstream region (see black dash circle). However, the second mode shape indicated that twisted flow can amplify the positive region near the left-side surface but shrink the negative area near the right-side surface, as indicated by the dashed rectangle in **Figure 9** (a_2) and (b_2). The possible reason could be that the conical vortex near the left side was enhanced but suppressed near the right side on the appearance of TWP.

The first two POD modes of the pressure field on the building surface for case CWP and TWP30 with 90°AOA was shown in **Figure 10**. Under CWP, a shift mode can also be observed for the first POD mode. Notably, the pressure pattern on the left and right sides are symmetrically distributed, but experiences an initially upward and then downward process from the windward edge to the leeward edge. Such finding indicates that flow separation and reattachment simultaneously occur at the side

(a_1) The first mode for CWP   (b_1) The first mode for TWP30

(a_2) The second mode for CWP   (b_2) The second mode for TWP30

Figure 9.
The first two POD modes of surface pressure field at 0°AOA for (a) CWP; (b) TWP30.

(a₁) The first mode for CWP   (b₁) The first mode for TWP30

(a₂) The second mode for CWP   (b₂) The second mode for TWP

Figure 10.
The first two POD modes of surface pressure field at 90°AOA for (a) CWP; (b) TWP30.

surface of the building with side ratio of 3:1. Similar to the 0°AOA case, the asymmetrical second mode of CWP is strongly related to the vortex shedding phenomenon. Affected by TWP, the continuous varying wind directions along the building height cause the reattachment location on the right-side surface to move upstream (see the red dash circle), however, that on the left-side surface becomes weaker (see blue dash circle). This observation indicates that the conical vortex near the left side is significantly weakened and merges into the wake flow. Overall, TWP has a distinctively different impact on the mode shape of buildings with different aspect ratios.

5. POD analysis of flow field

In this section, the wind incident angle of 0 degree is studied, which exactly corresponds to the side ratio case of 3:1, because in this case, the flow phenomenon is more complex. To identify the mechanisms that underlie the twisted-wind effect and elucidate the essential difference of the flow patterns under CWP and TWP, POD analysis was conducted on fluctuating velocity field at different horizontal planes (z = 1/6H, 1/2H and 5/6H) in the near-wake, and the spatial distribution and temporal evolution of the mode patterns were systematically compared for these two cases.

5.1 Mode energy contribution

Figure 11 shows the energy contributions of the dominant POD modes and cumulative energy of the first three modes. Under CWP, the kinetic energy contribution of the first two POD modes was the most prominent, and both exceeded 15%, while that of the third-order mode sharply decreased to below 10%. The largest cumulative energy proportion of the first three modes (46.71%) appeared at the middle plane $z = 1/2H$, where the coherent structure was less affected by the free end and the ground effect. This observation is consistent with the finding reported in [20]. Affected by the twisted flow, the energy proportion taken by main POD modes was relatively uniform, especially at the mid-height of the building, and for increasing height, the cumulative energy percentages of the first three main modes gradually decreased from 34.95% to 28.60%.

5.2 POD flow pattern

The first three POD mode patterns of wake velocity field into horizontal plane 1/2 H under CWP and TWP30 are depicted in **Figures 12** and **13** respectively. For CWP,


(a)

(b)

(c)
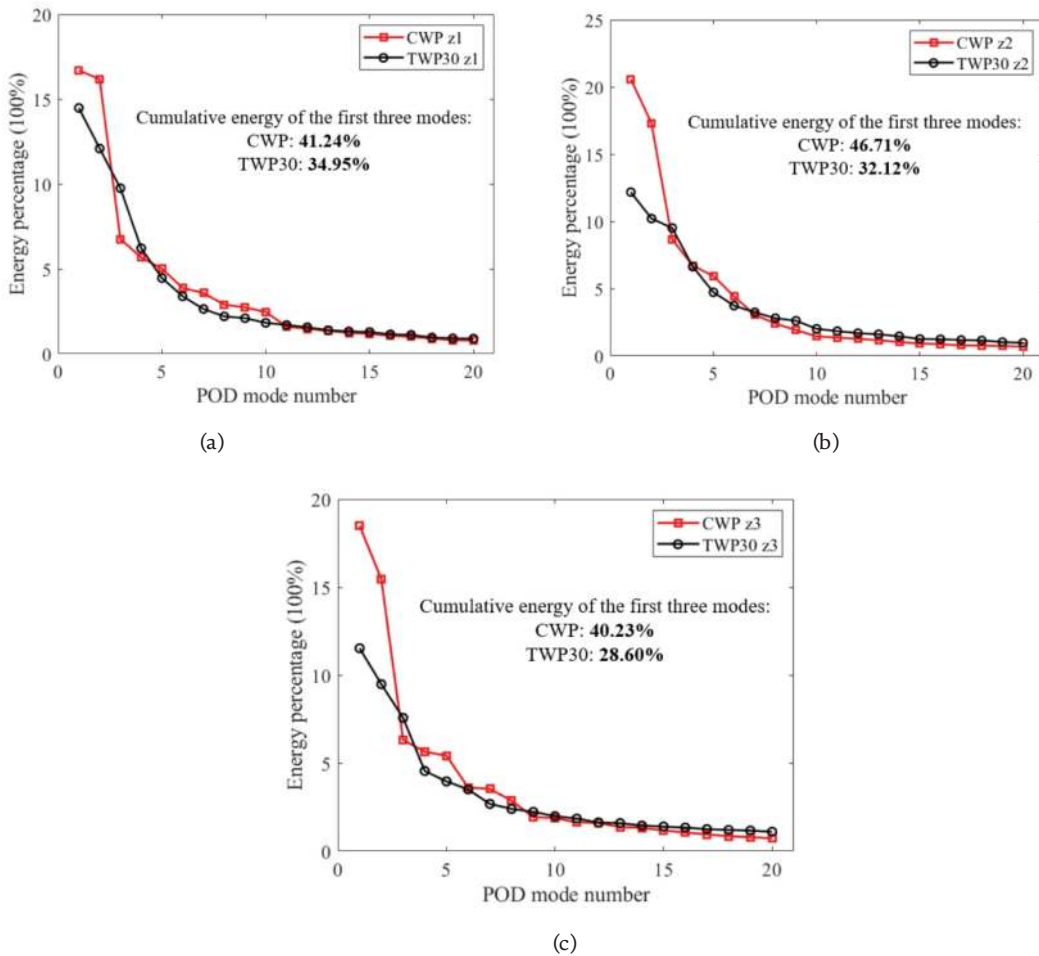
Figure 11.
Energy contributions of dominant POD modes and cumulative energy of the first three modes. (a) $z_1 = 1/6$ H. (b) $z_2 = 1/2$ H. (c) $z_3 = 5/6$ H.
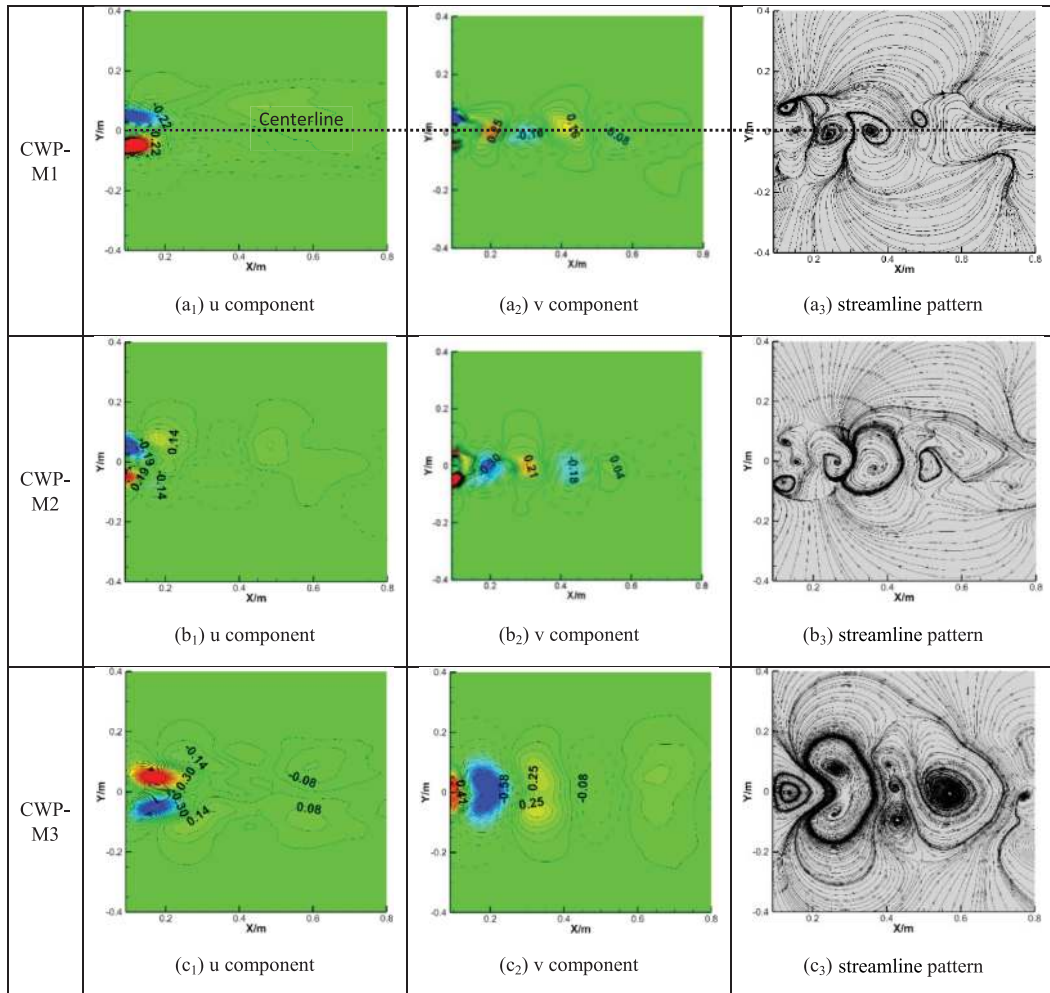
Figure 12.
The first three POD mode patterns of the wake velocity field at horizontal plane of 1/2 H under CWP (a) contour of u component; (b) contour of v component; (c) streamline pattern.

the contour of the u component was asymmetrically distributed while that of the v component was a symmetry to the centerline. The first two POD modes were similar (i.e., streamline pattern) but had an opposite sign, and as a result, can be recognized as a pair of conjugate modes. The third mode was found to have a series of vortices arrayed along the streamwise direction with alternating rotation direction. These observations confirm the findings reported in the previous POD investigation on the wake flow of a cylinder [27, 28].

To further disclose the temporal and spectral characteristics of the main underlying modes in the velocity fields, the PSD of the first three POD mode coefficients at the mid-height plane of the building were analyzed and compared for CWP and TWP30 as shown in **Figure 14**. As can be observed, there were several peaks for the first two POD modes while the most pronounced one appeared at f11 = 0.04 and f12 = 0.11(see blue arrow), these manifests that although coherent structures were composed of different sizes of vortices, the most dominant types were the LEVS and TEVS. The third mode had the main frequency of 0.11, and more importantly, its modal shape was regularly distributed and closely resembled the Karman vortex. Subsequently, it is reasonable to speculate that the third mode is highly related to the TEVS phenomenon.
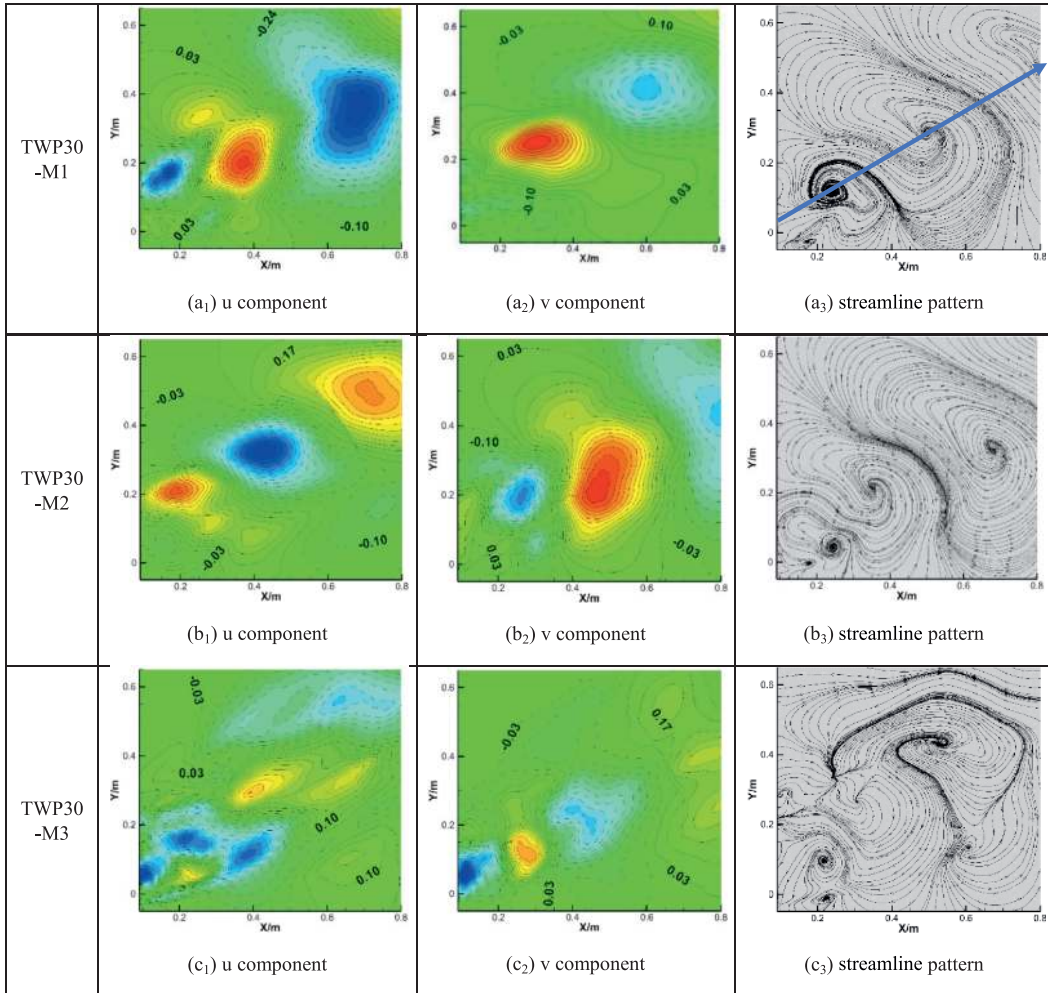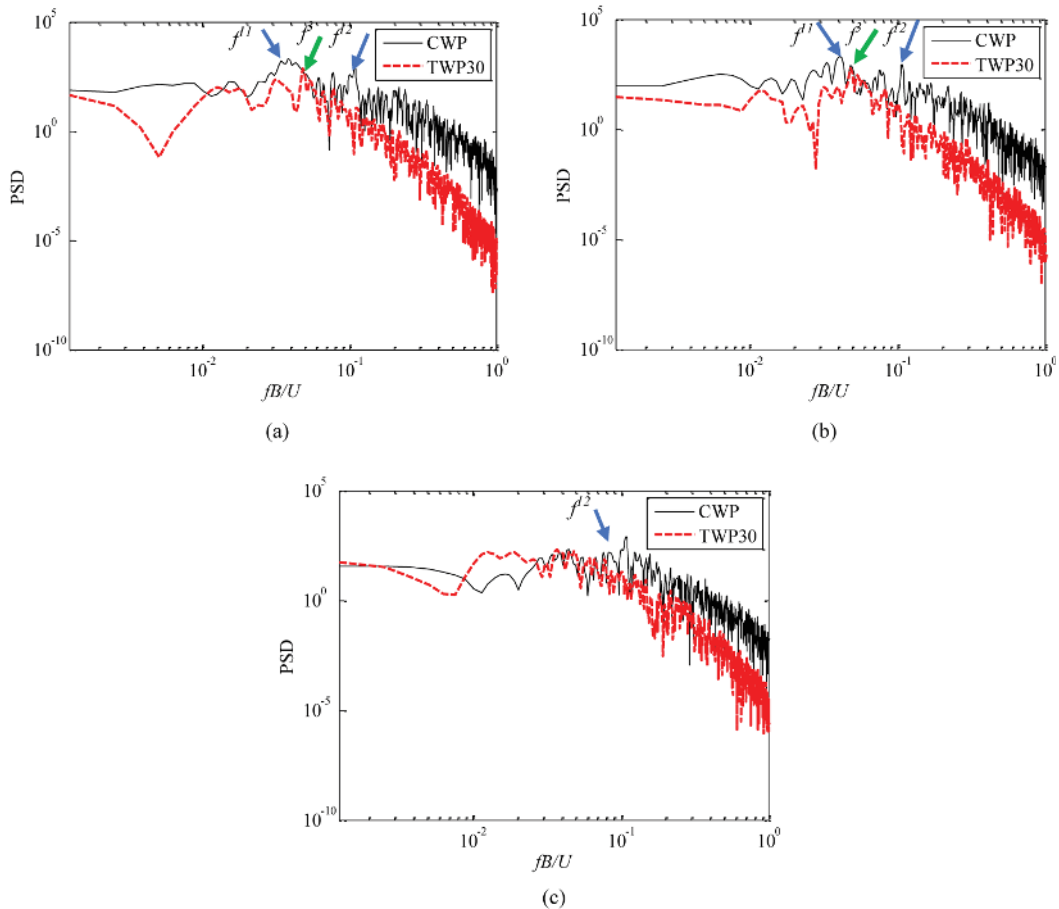
Figure 13.
The first three POD mode patterns of the wake velocity field at horizontal plane of 1/2 H under TWP30 (a) contour of u component; (b) contour of v component; (c) streamline pattern.

Under twisted flow, as shown in **Figure 13**, the mode topology and configuration were both largely modified, moreover, the vortex shedding was no longer aligned with the centerline but deviated towards the wind twisted direction. The vortex structures of the first two modes were very similar along and nearly had the same frequency of f3 = 0.048 (marked by green arrow in **Figure 13(c)**). This finding indicates that a pair of conjugate modes were well captured, with a high possibility to be controlled by the AEVS coherent structure. The twisted flow made the third mode shape less regular than that of CWP, and no distinctive peak was noted in this case.

To fully reveal the POD mode from a three-dimensional perspective, the mode results extracted from the velocity field at another horizontal plane z = 1/6 H under CWP and TWP30 are provided in **Figures 15** and **16**. It was found that the mode results at the plane near to the ground level z = 1/6 H basically shared a similar symmetrical distribution pattern to that of plane z = 1/6 H for the case of CWP and TWP30, despite some discrepancies (e.g., mode shape, magnitude and streamline) still being observed between these two horizontal planes due to the existence of the ground effect. An interesting observation is that because the twisted wind had a maximum twisted angle near the ground level, the twisted degree of the wake
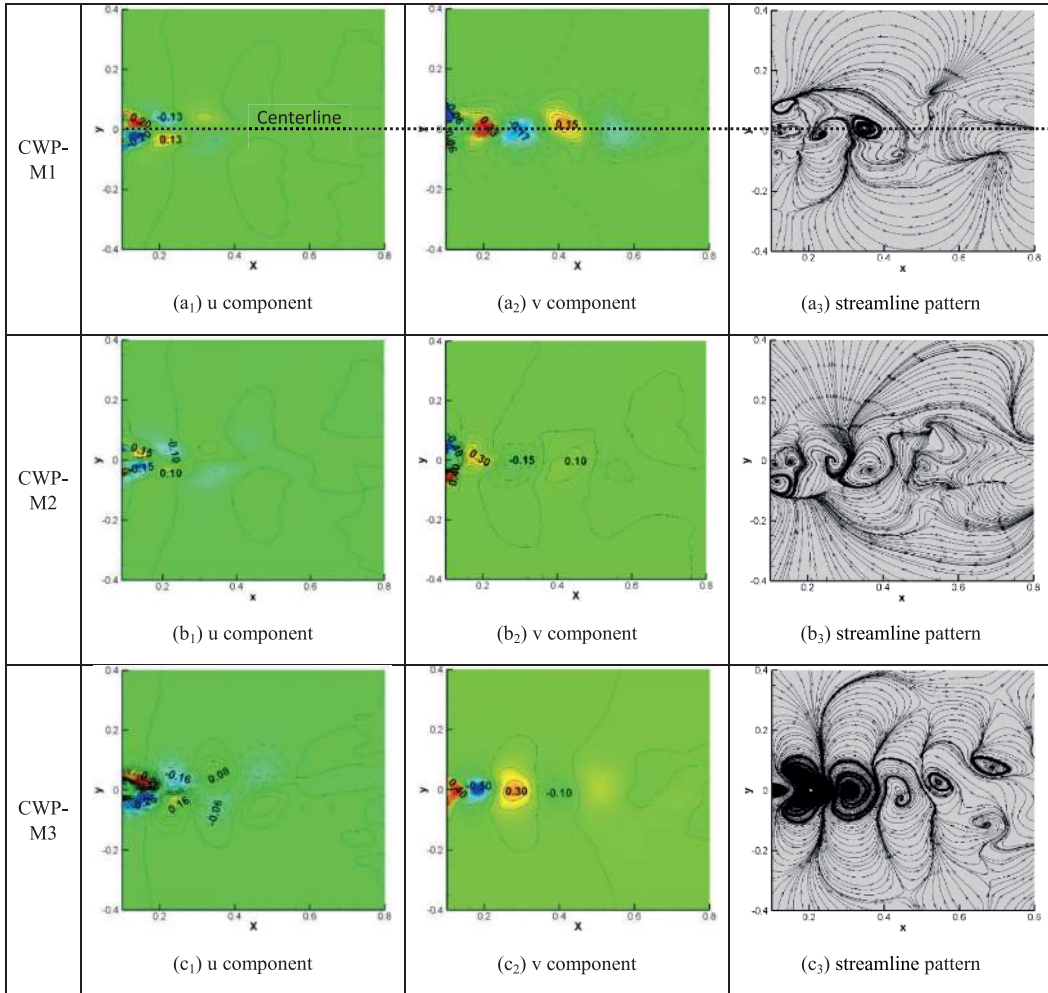
Figure 14.
Power spectral density of the first three modes for CWP and TWP30. (a) Mode 1. (b) Mode 2. (c). Mode 3.

streamline pattern was much larger in the horizontal plane of z = 1/6 H than that of plane of z = 1/2 H, as indicated by the blue arrow in **Figure 13**(a_3) and 16(a_3).

As can be seen in **Figures 15** and **16**, the distribution of mode pattern at the vertical plane x = 0.12 m exhibited symmetrical properties along the centerline y = 0 for the case of CWP, possibly related to the "quadrupole" wake pattern. In the case of TWP30, these POD modes deviated towards the approaching wind twisting direction, namely, the distribution was concentrated in the positive direction of the y-axis. It should be noted that in comparison with the CWP case, the distribution range and amplitude of the POD mode of w velocity were significantly amplified for the case of TWP30. This indicated that the interaction between the vertical velocity components at different heights in the flow field was more intense, which could explain the increase of the aerodynamic correlation of the local wind loads in the vertical direction.

5.3 Correlation of modal coefficients

Figure 17 shows the correlation of the first three POD mode coefficients at two horizontal planes (z_1 = 1/6H and z_2 = 1/2H) for CWP and TWP30.The x- and y-axis represent the modal coefficients of ith mode (i = 1,2 and 3) at the bottom height plane and mid-height plane respectively. For CWP, the phase-plane trajectory of the first three modes all exhibit a circular distribution (see the red dash line), thus, the
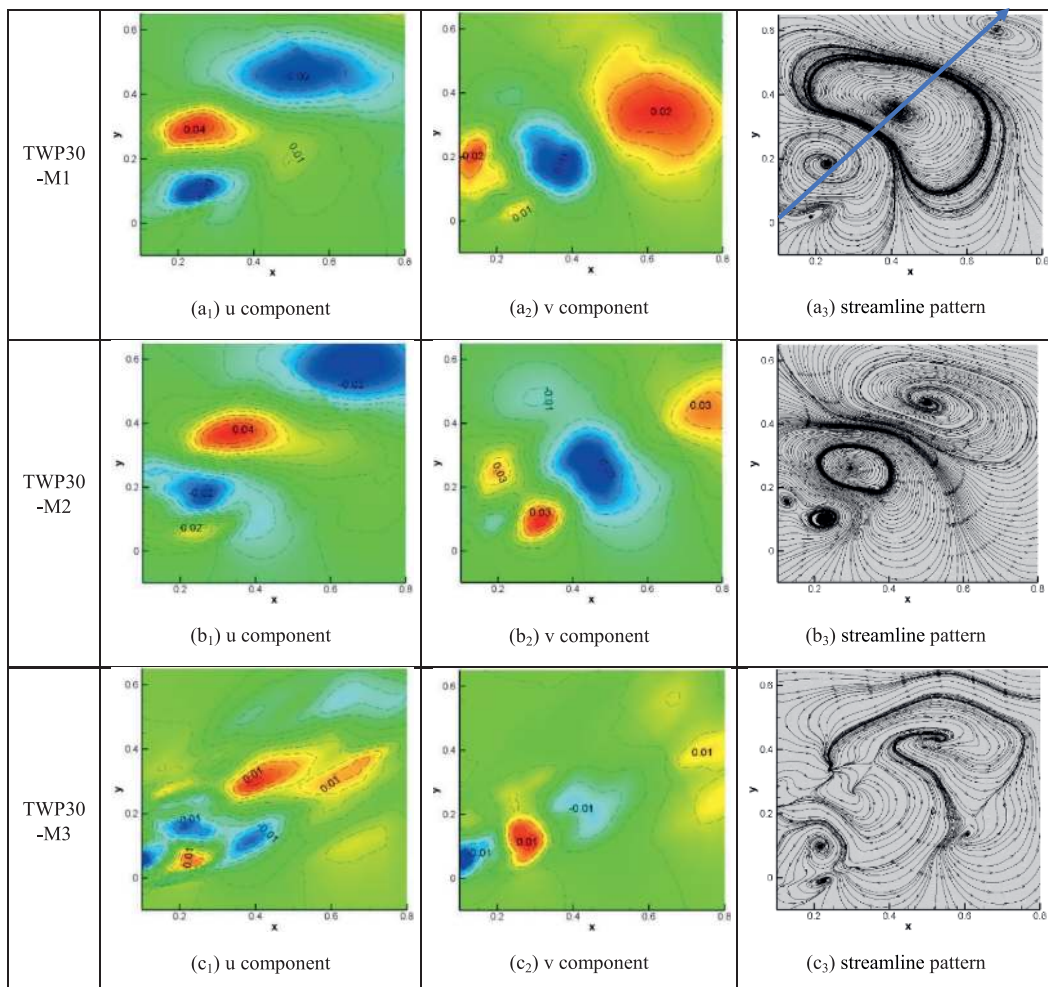
Figure 15.
The first three POD mode patterns of the wake velocity field at horizontal plane of 1/6 H under CWP (a) contour of u component; (b) contour of v component; (c) streamline pattern.

correlation of the same mode at different heights of the building is very close to zero, indicating that the coherent structure at these two locations is relatively independent. Conversely, affected by twisted flow, the distribution of the modal coefficients exhibits an inclined elliptic shape with a largely amplified correlation coefficient (see the black dash line). For example, the first predominant mode at these two different horizontal planes has the largest correlation coefficient *Cor* = 0.50, indicating that the predominant coherent structure simultaneously controls the flow motion at the bottom and middle planes. Notably, the correlation coefficients of the first mode (*Cor* = 0.50) and the second mode (*Cor* = 0.45) are very close to each other, demonstrating the existence of conjunction modes at the middle height of the building z_2 = 1/2H, as demonstrated in **Figure 17**(a_1) and (b_1).

6. Conclusions

This study aims to investigate the essential mechanism of nonlinear dynamic systems, i.e., the random pressure field and the flow field over a tall building

Figure 16.
The first three POD mode patterns of the wake velocity field at horizontal plane of 1/6 H under TWP30 (a) contour of u component; (b) contour of v component; (c) streamline pattern.

submerged in the turbulent boundary layer. The POD method is employed to extract the spatial/spectral features of the pressure pattern and flow pattern, and thus provides a physical mode interpretation of the aerodynamic characteristics of tall buildings subject to twisted winds. The primary conclusions are as follows:

1. POD can successfully extract the pressure mode and flow mode as well as capture the energy and spectral features of the dominant modes under the influence of CWP and TWP. The difference between the coherent structure in the twisted flow and the conventional flow is revealed, and the root cause of the influence of the twisted wind on the wind force and aerodynamic correlation of the high-rise building model is explained from the perspective of mode pattern.

2. For the pressure pattern, the first mode has a similar distribution to the mean pressure field, and is found to correspond to the low-frequency shift mode. While the second mode reveals various vortex shedding phenomena (i.e., Karman vortex, LEVS, TEVS, AVES) for the 0°and 90° cases. Compared with CWP, TWP largely modifies the pressure distribution, the power spectral feature
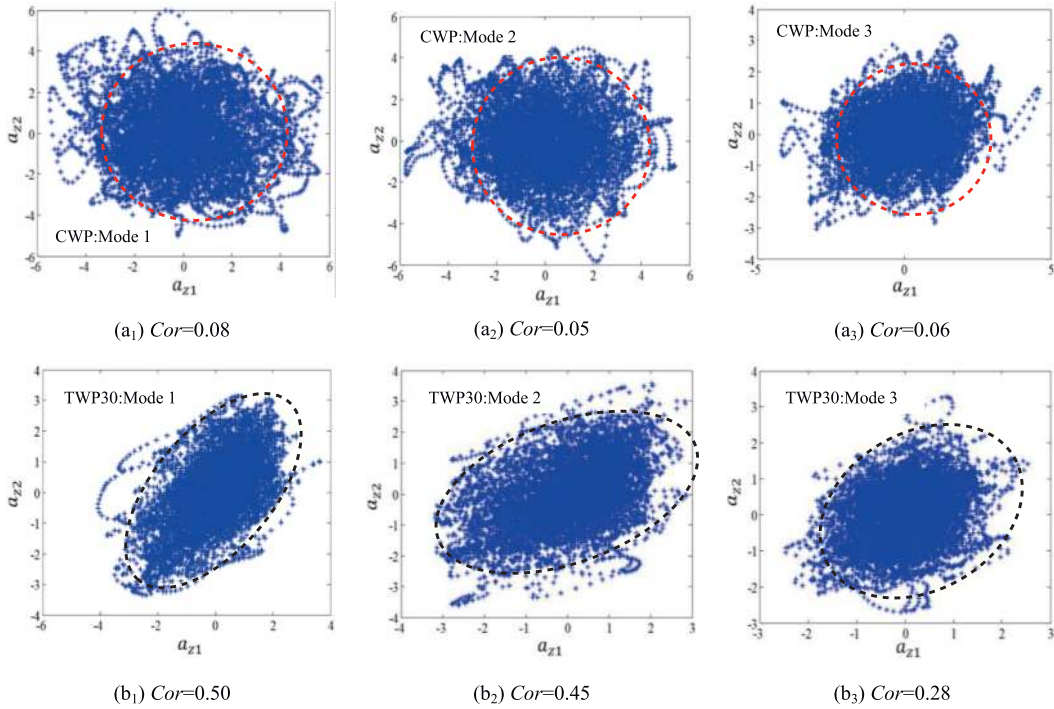
Figure 17.
Correlation of the first three POD mode coefficients of two horizontal planes at height of z = 1/6H and 1/2H for (a) CWP; (b) TWP30.

and the energy proportion of the dominant modes, and this modification in the POD mode pattern causes the twisted flow to have a significantly different impact on the aerodynamic properties of buildings. Specifically,

    i. In the case of 0°AOA, when exposed to CWP, the first mode pattern has a similar distribution to the mean pressure field, implying that the first POD mode corresponds to the low-frequency shift mode. Whereas the second mode shape presents the asymmetrical feature, which possibly reflects the fluctuating properties induced by the periodic wake shedding. In the presence of twisted wind, the POD mode pattern on building surfaces is significantly modified, whose distribution appears more asymmetric and non-uniform. It is evident that the vertical varying wind direction has a more noticeable influence on the mode shape on the leeward surface than on the windward surface. Specifically, the first mode shape severely deflects towards the right side near the downstream region, while the second mode shape indicates that twisted flow could amplify the positive region near the left-side surface but shrink the negative area near the right-side surface. Such phenomena could be also observed for the second mode shape distributed on the side surfaces. This observation demonstrates that the conical vortex near the left side is greatly enhanced while it is largely suppressed near the right side, as highlighted by the black circle.

    ii. In the case of 90°, under CWP, a shift mode is also observed for the first POD mode. Notably, the pressure pattern on the left and right sides are

symmetrically distributed, but experience an initially upward and then downward process from the windward edge to the leeward edge. Such finding indicates that flow separation associated with flow reattachment simultaneously occurs at the side surface of a building with a large side ratio of 3:1. Similar to the 0° wind incident angle case, the asymmetrical second mode of CWP is highly related to the vortex shedding phenomenon. Affected by TWP, the continuous varying wind directions along the building height cause the reattachment location on the right-side surface moves forward, while that on the left-side surface basically disappears. Overall, the TWP has a similar influence on the mode shape of the windward and leeward surfaces for buildings attacked by 0°and 90° approaching wind.

3. For the flow pattern, its spatial–temporal features under CWP and TWP are successfully captured by POD. The main mode pattern of CWP is found to be controlled by the ILEVS and TEVS phenomenon, which corresponds to frequencies of f_{11} = 0.04 and f_{12} = 0.102 respectively. Whereas, the predominant POD mode of TWP is highly related to AEVS with a frequency of f_3 = 0.048. This modal pattern is reported to twist towards the wind direction with a more regular shape, even though it becomes less intense. Moreover, the spanwise correlation of the main POD mode at two planes of different heights is also significantly enhanced by TWP.

The study has comprehensively revealed the potential mechanisms of the twisted-wind effect that underlies the pressure field and flow field of tall buildings exposed to TWP. The mode interpretation of aerodynamic characteristics is expected to shed light on the fluid-induced interaction between twisted flows and tall buildings, and provides a better understanding of the underlying mechanism of the twisted-wind effect. The obtained conclusions facilitate useful references for designing and constructing tall buildings in hilly terrain where twisted wind occurs frequently, and more importantly, for TWP-induced vibration control measures.

Acknowledgements

Nomenclature

AOA	Angle of attack
ABL	Atmospheric boundary layer
CWP	Conventional wind profile
TWP	Twisted wind profile
MTA	Maximum twisted angle at ground level
POD	Proper orthogonal decomposition
ROMs	Reduced-order models
SMPSS	Synchronous multi-pressure sensing system

Author details

Lei Zhou and Kam Tim Tse*
Department of Civil and Environmental Engineering, The Hong Kong University of
Science and Technology, Clear Water Bay, Kowloon, Hong Kong, China

*Address all correspondence to: timkttse@ust.hk

IntechOpen

References

[1] Weerasuriya AU, Hu ZZ, Zhang XL, Tse KT, Li S, Chan PW. New inflow boundary conditions for modeling twisted wind profiles in CFD simulation for evaluating the pedestrian-level wind field near an isolated building. Building and Environment. 2018a;**132**:303-318

[2] Weerasuriya AU, Tse KT, Zhang X, Kwok KCS. Equivalent wind incidence angle method: A new technique to integrate the effects of twisted wind flows to AVA. Building and Environment. 2018b;**139**:46-57

[3] Tse K-T, Weerasuriya AU, Zhang X, Li S, Kwok KCS. Pedestrian-level wind environment around isolated buildings under the influence of twisted wind flows. Journal of Wind Engineering and Industrial Aerodynamics. 2017a;**162**: 12-23

[4] Tse K-T, Weerasuriya AU, Zhang X, Li SW, Kwok KCS. Effects of twisted wind flows on wind conditions in passages between buildings. Journal of Wind Engineering and Industrial Aerodynamics. 2017b;**167**:87-100

[5] Liu Z, Zheng C, Wu Y, Flay RGJ, Zhang K. Investigation on the effects of twisted wind flow on the wind loads on a square section megatall building. Journal of Wind Engineering and Industrial Aerodynamics. 2019a;**191**:127-142

[6] Liu Z, Zheng C, Wu Y, Flay RGJ, Zhang K. Wind tunnel simulation of wind flows with the characteristics of thousand-meter high ABL. Building and Environment. 2019b;**152**:74-86

[7] Feng C, Gu M, Zheng D. Numerical simulation of wind effects on super high-rise buildings considering wind veering with height based on CFD. Journal of Fluids and Structures. 2019;**91**:102715

[8] Zhou L, Hu G, Tse KT, He X. Twisted-wind effect on the flow field of tall building. Journal of Wind Engineering and Industrial Aerodynamics. 2021a;**218**:104778

[9] Zhou L, Tse KT, Hu G, Li Y. Higher order dynamic mode decomposition of wind pressures on square buildings. Journal of Wind Engineering and Industrial Aerodynamics. 2021;**211**:104545

[10] Zhou L, Tse KT, Hu G, Li Y. Mode interpretation of interference effects between tall buildings in tandem and side-by-side arrangement with POD and ICA. Engineering Structures. 2021b;**243**: 112616

[11] Ding F, Kareem A. Tall buildings with dynamic facade under winds. Engineering. 2020;**6**:1443-1453

[12] Nankai K et al. Linear reduced-order model based on PIV data of flow field around airfoil. Transactions of the Japan Society forAeronautcal and Space Sciences. 2019;**62**:227-235

[13] Kareem A. Mapping and synthesis of random pressure fields. Journal of Engineering Mechanics-Asce. 1989;**115**: 2325-2332

[14] Chen XZ, Kareem A. Proper orthogonal decomposition-based modeling, analysis, and simulation of dynamic wind load effects on structures. Journal of Engineering Mechanics. 2005; **131**:325-339

[15] Sirovich L. Turbulence and the dynamics of coherent structures. 1. Coherent Structures. Quarterly of Applied Mathematics. 1987;**45**:561-571

[16] Baker CJ. Aspects of the use of proper orthogonal decomposition of

surface pressure fields. Wind and Structures. 2000;**3**:97-115

[17] Bastine D et al. Stochastic wake modelling based on POD analysis. Energies. 2018;**11**(3):612

[18] Carassale L, Brunenghi MM. Statistical analysis of wind-induced pressure fields: A methodological perspective. Journal of Wind Engineering Industrial Aerodynamics. 2011;**99**:700-710

[19] Tamura Y et al. Proper orthogonal decomposition of random wind pressure field. Journal of Fluid Structure. 1999;**13**: 1069-1095

[20] Wang F, Lam KM. Geometry effects on mean wake topology and large-scale coherent structures of wall-mounted prisms. Physics of Fluids. 2019;**31**:125109

[21] Wang HF, Cao HL, Zhou Y. POD analysis of a finite-length cylinder near wake. Experiments in Fluids. 2014;**55**: 1790

[22] Tse K-T, Weerasuriya AU, Kwok KCS. Simulation of twisted wind flows in a boundary layer wind tunnel for pedestrian-level wind tunnel tests. Journal of Wind Engineering and Industrial Aerodynamics. 2016;**159**:99-109

[23] Yu Y, Yang Y, Xie Z. A new inflow turbulence generator for large eddy simulation evaluation of wind effects on a standard high-rise building. Building and Environment. 2018;**138**:300-313

[24] Van Doormaal JP, Raithby GD. Enhancements of the SIMPLE method for predicting incompressible fluid flows. Numerical Heat Transfer. 1984;**7**: 147-163

[25] Deniz S, Staubli T. Oscillating rectangular and octagonal profiles:

Interaction of leading-and trailing-edge vortex formation. Journal of Fluids and Structures. 1997;**11**:3-31

[26] Zhang H, Xin D, Ou J. Wake control using spanwise-varying vortex generators on bridge decks: A computational study. Journal of Wind Engineering and Industrial Aerodynamics. 2019;**184**:185-197

[27] Schmid PJ. Dynamic mode decomposition of numerical and experimental data. Journal of Fluid Mechanics. 2010;**656**:5-28

[28] Zhang Q, Liu Y, Wang S. The identification of coherent structures using proper orthogonal decomposition and dynamic mode decomposition. Journal of Fluids and Structures. 2014; **49**:53-72